


# Tuning Plasmonic Properties of Truncated Gold Nanospheres by Coating

Sergey Scherbak<sup>1,2</sup> · Nikolai Kapralov<sup>2</sup> · Igor Reduto<sup>1,2,3</sup>  · Semyon Chervinskii<sup>2,3</sup> · Olga Svirko<sup>3</sup> · Andrey Lipovskii<sup>1,2</sup>

Received: 12 August 2016 / Accepted: 25 November 2016 / Published online: 6 December 2016  
© Springer Science+Business Media New York 2016

**Abstract** The influence of TiO<sub>2</sub> coating on resonant properties of gold nanoisland films deposited on silica substrates was studied numerically and in experiments. The model describing plasmonic properties of a metal truncated nanosphere placed on a substrate and covered by a thin dielectric layer has been developed. The model allows calculating a particle polarizability spectrum and, respectively, its surface plasmon resonance (SPR) wavelength for any given cover thickness, particle radius and truncation parameter, and dielectric functions of the particle, the substrate, the coating layer, and the surrounding medium. Dependence of the SPR position calculated for truncated gold nanospheres has coincided with the measured one for the gold nanoisland films covered with titania of different thicknesses. In the experiments, gold films with thickness of 5 nm were deposited on a silica glass substrate, annealed at 500 °C to form nanoislands of 20 nm in diameter, and covered with amorphous titania layers using atomic layer deposition technique. The resulting structures were characterized with scanning electron microscopy and optical absorption spectroscopy. The measured dependence of the SPR position on titania film thickness corresponded to the one calculated

for truncated sphere-shaped nanoparticles with the truncation angle of ~50°. We demonstrated the possibility of tuning the SPR position within ~100 nm range by depositing to 30 nm thick titania layer.

**Keywords** Nanoisland film · Truncated gold nanospheres · Titania cover · Atomic layer deposition · Surface plasmon resonance

## Introduction

Nanoparticles and nanoisland films of noble metals have demonstrated their applicability in sensing [1–3], surface-enhanced Raman scattering (SERS) [4], second harmonic generation [5, 6], catalysis, photovoltaics, and solar cells [7–9]. Broad application area is possible due to surface plasmon resonance (SPR) in the visible range of wavelengths: blue for silver and green for gold and copper nanoparticles. Gold nanoparticles are of interest for many areas because of their chemical stability. Since most of the applications are based on the SPR phenomenon, it is required to develop techniques to manipulate SPR wavelength. Generally, characteristics of surface plasmons in nanoparticles of particular metal depend on the shape and size of the nanoparticles [10–12] and on their surrounding [13–15]. Layers of spherical gold nanoparticles can be prepared by precipitation from aqueous solutions on various substrates [16], in particular, on etched glass surfaces [17]. Another technique is based on thermal treatment of thin gold films produced by thermal evaporation or sputtering [18]. The annealing leads to the disaggregation of the film into particles [19–21], which is driven by the minimization of surface energy [22]. Generally, both techniques suffer from the poor adhesion of the nanoparticles to the substrate [23]; however, flat bottom of the nanoparticles formed from metal films [24, 25] should

**Electronic supplementary material** The online version of this article (doi:10.1007/s11468-016-0461-5) contains supplementary material, which is available to authorized users.

✉ Igor Reduto  
reduto-igor@mail.ru

<sup>1</sup> St. Petersburg Academic University, 8/3 Khlopina, St. Petersburg 194021, Russia

<sup>2</sup> Peter the Great St. Petersburg Polytechnic University, 29 Polytechnicheskaya, St. Petersburg 195251, Russia

<sup>3</sup> University of Eastern Finland, P.O. Box 111, FI-80101 Joensuu, Finland

result in slightly better adhesion of such nanoparticles to substrates in comparison with spherical nanoparticles [16] prepared from solutions. This is because of smaller nanoparticle-substrate contact area and, correspondingly, lower Van der Waals bonding energy in the latter case. According to Gupta and co-authors [24], the nanoparticles formed from a gold film were found to have merits over the commonly used gold colloid films such as easier and inexpensive fabrication and high island density without agglomeration. It has been shown that this approach results in the formation of nanoparticles shaped as truncated spheres [24], between hemispherical and spherical. Because of difficulties in precise characterizing the shape of nanometer-scale particles falling between a hemisphere and a sphere, Tian et al. (2014) [25] indirectly identified the shape basing on the comparison of electrodynamic modeling with resonant wavelengths of plasmons measured using s- and p-polarized optical excitation. This study allowed establishing the correlation between the thickness of a gold film deposited onto a silica substrate, the temperature of annealing, and the sphere truncation angle. The shape of the nanoparticles transformed towards spherical with the increase in annealing temperature from 500 to 900 °C, and in case of s-polarized excitation, this corresponded to the shift of the SPR wavelength from 550 to 525 nm for gold evaporated effective thickness of 5 nm. We have recently presented the model describing the controllable shift of the SPR wavelength in hemispherical metal nanoparticles on a substrate via depositing high-index film [26] and verified this in the experiments on manipulating the SPR wavelength in silver nanoparticles covered with titania using atomic layer deposition (ALD) [13]. The tuning of the SPR wavelength to particular light sources and, in sensing (e.g., using SERS), to analytes [13, 25] provides enhancement of the resonant electric field and related phenomena in a desirable spectral range. Here, we present the model of resonant properties of truncated plasmonic nanospheres under thin film cover and the results of our experiments with gold nanoparticles covered with titania layers of different thicknesses. We show that thin film covering these truncated metal nanospheres allows controlling their SPR position in a wide range. Using the set of coatings with different thicknesses, it was also possible to evaluate the shape of the nanoparticles that is the truncation angle.

## Experimental

To fabricate gold nanoisland films, we used thermal evaporation and sputtering of gold material on silica substrates (substrate refractive index  $n = 1.48$  and it is weakly dispersive in optical range) with subsequent thermal annealing of deposited Au film. In preliminary deposition experiments, we used fast and simple sputtering method with Emitech K675X (Emitech Ltd, England) under  $10^{-3}$  Pa vacuum. For film deposition with

better surface uniformity, we used thermal evaporation method with Leybold Heraeus Univex 300 (Oerlikon Leybold Vacuum, Germany) under  $10^{-5}$  Pa vacuum. In both experiments, target effective thickness of deposited gold films was 5 nm.

For the growth of gold nanoislands from the deposited gold layer, we used thermal annealing similarly to the process used for the formation of gold nanoislands on mica substrate [27]. The samples were annealed in air atmosphere for 60–300 min at 300–500 °C.

We used scanning electron microscopy (SEM; Leo 1550 Gemini, Oberkochen, Germany) for imaging of deposited and annealed gold films to characterize geometrical shape and the sizes of nanoislands. Electron beam voltage was chosen between 2 and 5 kV to optimize resolution and contrast with the charging samples. The scale bar redrawn with CorelDraw software for better readability was added to original SEM images.

Optical absorption spectra were measured for samples with initial gold films, annealed gold nanoislands, and covered with TiO<sub>2</sub> gold nanoisland films. We performed the measurements in a spectral range from 300 to 1100 nm with 1 nm wavelength steps using spectrophotometer Specord 50 (Analytik Jena AG, Jena, Germany) for all samples.

To coat the gold nanoislands with thin layers of titanium dioxide, we employed atomic layer deposition (ALD). TiO<sub>2</sub> was chosen for its high refractive index ( $n = 2–2.5$  in 550–650 nm region depending on chosen deposition technique [28, 29]) strongly influencing to the SPR wavelength. Titania films were deposited at 120 °C in Beneq TFS-200 reactor (Beneq Oy, Espoo, Finland) using titanium tetrachloride (TiCl<sub>4</sub>) and water (H<sub>2</sub>O) precursors, with a nitrogen purge after each deposition cycle. We deposited six layers of different thicknesses, which was initially estimated by the number of deposition cycles.

The thickness and refractive index of the deposited titania films were verified using a variable angle spectroscopic ellipsometer VASE® with a High-Speed Monochromator System HS-190TM (J.A. Woollam Co., Lincoln, NE, USA); the beam spot size of 1 mm was used.

## Modeling

In accordance with Ref. 24, gold nanoislands formed on a fused silica surface via annealing of the deposited gold film have a truncated sphere shape, the truncation angle being dependent on the annealing conditions. Except the type of metal, optical polarizability of such nanoparticles depends on the truncation angle, on the dielectric permittivity of substrate and cover materials, and on the thickness of the covering layer. To calculate the polarizability dispersion of the truncated sphere placed on a dielectric substrate and covered by a

dielectric layer of a finite thickness, we based on the approach originally proposed by Wind et al. (1987) [30]. In that paper, the authors presented a semi-analytical study of the polarizability of a truncated spherical nanoparticle on a dielectric substrate. Here, we broaden this approach to the case of a layer of finite thickness placed between the particle and a surrounding medium and analyze how the layer influences the particle resonant properties.

We consider a truncated sphere of radius  $R$  with a dispersive dielectric function  $\epsilon_5(\omega)$  placed on a substrate with dielectric constant  $\epsilon_2$ (Fig. 1). The distance from the sphere center to the substrate surface is  $H$ . The particle is covered by a layer of thickness  $h$  and dielectric constant  $\epsilon_3$ . Shape of the coating layer is assumed to replicate shape of the particle, which is a truncated sphere; this coating conformality is known to be typical for ALD [13, 31]. The dielectric constant of outer surrounding medium is  $\epsilon_1$ . In addition, as was mentioned by Tian et al. (2014) [25], it is convenient to consider regions 4 and 6 in the substrate (Fig. 1) having different dielectric constants  $\epsilon_4$  and  $\epsilon_6$ , respectively. This allows studying only the case when the center of the truncated sphere lies above the substrate surface. The opposite case can be solved by simple switching  $\epsilon_1$  and  $\epsilon_2$ ,  $\epsilon_3$  and  $\epsilon_4$ ,  $\epsilon_5$  and  $\epsilon_6$ , respectively. Note that spectral dependencies of  $\epsilon_{1-4}$  and  $\epsilon_6$  can be taken into consideration, if needed, but in frames of the present study it is not crucial.

Typical particles have size of several tens of nanometers (see Fig. 2b below in the “Results and Discussion” section) that is much less than the wavelength of the incident light, and this allows using so-called quasistatic (dipole) approximation [32]. In the dipole approximation, any phase retardation of the external electric field can be neglected, and one can solve the Laplace equation instead of finding full-field solution of the Helmholtz equation. Thus, in this approximation, we can consider the particle being under a homogeneous external electric field,  $E_{ext}$ . Wind et al. (1987) [30] consider a general case when the external field has both components: normal and along the substrate surface. To avoid overloading the following equations, we consider the case when the external field is

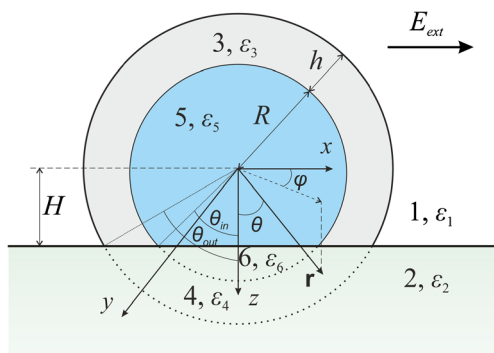


**Fig. 1** Scheme of the dielectric covered truncated nanoparticle (color online)

parallel to the substrate surface. This corresponds to a typical case of normal light incidence and is of interest for the comparison with the spectroscopic results.

We can write expressions for reduced (normalized by  $-E_{ext}R$ ) potential in each region through the expansion by the eigenfunctions of the Laplace operator in the spherical coordinate system:

$$\psi_1 = r \sin \theta \cos \varphi + \sum_{j=1}^{\infty} r^{-j-1} B_1^j P_j^1(\cos \theta) \cos \varphi + \sum_{j=1}^{\infty} \hat{B}_1^j V_j^1(r, \cos \theta) \cos \varphi \tag{1a}$$

$$\psi_2 = r \sin \theta \cos \varphi + \sum_{j=1}^{\infty} r^{-j-1} B_2^j P_j^1(\cos \theta) \cos \varphi \tag{1b}$$

$$\psi_3 = \sum_{j=1}^{\infty} [r^j A_3^j + r^{-j-1} C_3^j] P_j^1(\cos \theta) \cos \varphi + \sum_{j=1}^{\infty} [\hat{A}_3^j W_j^1(r, \cos \theta) + \hat{C}_3^j V_j^1(r, \cos \theta)] \cos \varphi \tag{1c}$$

$$\psi_4 = \sum_{j=1}^{\infty} [r^j A_4^j + r^{-j-1} C_4^j] P_j^1(\cos \theta) \cos \varphi \tag{1d}$$

$$\psi_5 = \sum_{j=1}^{\infty} r^j B_5^j P_j^1(\cos \theta) \cos \varphi + \sum_{j=1}^{\infty} \hat{B}_5^j W_j^1(r, \cos \theta) \cos \varphi \tag{1e}$$

$$\psi_6 = \sum_{j=1}^{\infty} r^j B_6^j P_j^1(\cos \theta) \cos \varphi \tag{1f}$$

where

$$V_j^1(r, \cos \theta) = (r^2 - 4rr_0 \cos \theta + 4r_0^2)^{-\frac{j-1}{2}} P_j^1 \left( \frac{r \cos \theta - 2r_0}{\sqrt{(r^2 - 4rr_0 \cos \theta + 4r_0^2)}} \right) \tag{2a}$$

$$W_j^1(r, \cos \theta) = (r^2 - 4rr_0 \cos \theta + 4r_0^2)^{\frac{j}{2}} P_j^1 \left( \frac{r \cos \theta - 2r_0}{\sqrt{(r^2 - 4rr_0 \cos \theta + 4r_0^2)}} \right) \tag{2b}$$

$P_j^1(\cos \theta)$  is the first associated Legendre polynomial of the  $j$ th order;  $r_0 = \frac{H}{R}$  is a truncation parameter;  $r$ ,  $\theta$ , and  $\varphi$  are spherical coordinates depicted in Fig. 1 ( $r$  is also normalized by  $R$ ). The potential subscripts denote which region it relates to. Essentially, Eqs. 1a–f correspond to multipole expansion.

Factors  $B_{1-2,5-6}^j$ ,  $\hat{B}_{1-2,5-6}^j$ ,  $A_{3,4}^j$ ,  $C_{3,4}^j$ ,  $\hat{A}_{3,4}^j$ , and  $\hat{C}_{3,4}^j$  are unknown expansion coefficients which are to be found. The terms outside the sum in Eqs. 1a,b relate to the external potential. The terms, which contain functions  $W_j^1(r, \cos\theta)$  and  $V_j^1(r, \cos\theta)$ , describe the substrate influence and correspond to the multipole mirror image in the substrate. Note that in the expansions 1a–f, we tacitly used only those spherical functions, which contain  $\cos\varphi$  as an azimuth dependence. The axial symmetry of the problem forbids any other azimuth dependencies but the ones appear in the external potential, e.g.,  $\cos\varphi$  as in the considered case. Also, we used the condition of the potential finiteness at  $r \rightarrow 0$  and  $r \rightarrow \infty$ . That is why the potentials outside the sphere and the coating,  $\psi_1$  and  $\psi_2$ , contain only the negative powers of  $r$ , and inside potentials,  $\psi_5$  and  $\psi_6$ , contain only the positive powers of  $r$ . Nonetheless, both terms with  $r^j$  and  $r^{-j-1}$  appear in the expansion of the potentials in the covering layer,  $\psi_3$  and  $\psi_4$ .

Standard boundary conditions, which are the continuity of both the potential and the normal component of the electric displacement, at the surface of the substrate (boundaries 1–2, 3–4, and 5–6) lead to the relations between coefficients:

$$\begin{aligned} B_{2,6}^j &= \frac{2\varepsilon_{1,5}}{\varepsilon_{1,5} + \varepsilon_{2,6}} B_{1,5}^j, & \hat{B}_{1,5}^j &= (-1)^{j+1} \frac{\varepsilon_{1,5} - \varepsilon_{2,6}}{\varepsilon_{1,5} + \varepsilon_{2,6}} B_{1,5}^j \\ A_4^j &= \frac{2\varepsilon_3}{\varepsilon_3 + \varepsilon_4} A_3^j, & \hat{A}_3^j &= (-1)^{j+1} \frac{\varepsilon_3 - \varepsilon_4}{\varepsilon_3 + \varepsilon_4} A_3^j \\ C_4^j &= \frac{2\varepsilon_3}{\varepsilon_3 + \varepsilon_4} C_3^j, & \hat{C}_3^j &= (-1)^{j+1} \frac{\varepsilon_3 - \varepsilon_4}{\varepsilon_3 + \varepsilon_4} C_3^j \end{aligned} \quad (3)$$

Next we use boundary conditions on the surface of the spheres (boundaries 1–3, 3–5, 2–4, and 4–6). We keep in the expansions 1a–f finite number of terms  $N$ , substitute the series in the boundary conditions, multiply each equation by  $P_k^1(\cos\theta) \cos\varphi \sin\theta$ , and integrate over  $\theta$  from  $-\pi$  to  $\pi$  and over  $\varphi$  from 0 to  $2\pi$ . The resulted equations in general form are as follows:

$$\int_{-1}^{r_0} dt \int_0^{2\pi} d\varphi [\psi_3 - \psi_5]_{r=1} P_k^1(t) \cos\varphi + \int_{r_0}^1 dt \int_0^{2\pi} d\varphi [\psi_3 - \psi_5]_{r=1+h} P_k^1(t) \cos\varphi = 0 \quad (4a)$$

$$d\varphi [\psi_4 - \psi_6]_{r=1} P_k^1(t) \cos\varphi = 0$$

$$\int_{-1}^{r_0} dt \int_0^{2\pi} d\varphi \left[ \varepsilon_3 \frac{\partial \psi_3}{\partial r} - \varepsilon_5 \frac{\partial \psi_5}{\partial r} \right]_{r=1} P_k^1(t) \cos\varphi + \int_{r_0}^1 dt \int_0^{2\pi} d\varphi \left[ \varepsilon_3 \frac{\partial \psi_3}{\partial r} - \varepsilon_5 \frac{\partial \psi_5}{\partial r} \right]_{r=1+h} P_k^1(t) \cos\varphi = 0 \quad (4b)$$

$$d\varphi \left[ \varepsilon_4 \frac{\partial \psi_4}{\partial r} - \varepsilon_6 \frac{\partial \psi_6}{\partial r} \right]_{r=1} P_k^1(t) \cos\varphi = 0$$

$$\int_{-1}^{\hat{r}_0} dt \int_0^{2\pi} d\varphi [\psi_1 - \psi_3]_{r=1+h} P_k^1(t) \cos\varphi + \int_{\hat{r}_0}^1 dt \int_0^{2\pi} d\varphi [\psi_1 - \psi_3]_{r=1+h} P_k^1(t) \cos\varphi = 0 \quad (4c)$$

$$d\varphi [\psi_1 - \psi_3]_{r=1+h} P_k^1(t) \cos\varphi = 0$$

$$\int_{-1}^{\hat{r}_0} dt \int_0^{2\pi} d\varphi \left[ \varepsilon_1 \frac{\partial \psi_1}{\partial r} - \varepsilon_3 \frac{\partial \psi_3}{\partial r} \right]_{r=1} P_k^1(t) \cos\varphi + \int_{\hat{r}_0}^1 dt \int_0^{2\pi} d\varphi \left[ \varepsilon_1 \frac{\partial \psi_1}{\partial r} - \varepsilon_3 \frac{\partial \psi_3}{\partial r} \right]_{r=1+h} P_k^1(t) \cos\varphi = 0 \quad (4d)$$

$$d\varphi \left[ \varepsilon_1 \frac{\partial \psi_1}{\partial r} - \varepsilon_3 \frac{\partial \psi_3}{\partial r} \right]_{r=1+h} P_k^1(t) \cos\varphi = 0$$

Here,  $\hat{r}_0 = \frac{r_0}{1+h}$  and thickness  $h$  is normalized by radius  $R$ ,  $\hat{r}_0 = \cos\theta_{\text{out}}$  and  $r_0 = \cos\theta_{\text{in}}$  where  $\theta_{\text{in}}$  and  $\theta_{\text{out}}$  are truncation angles of the sphere and the shell, respectively. Substituting the expressions for  $\psi_{1-6}$  in Eqs. 4a–d leads to the system of  $4N$  equations which solution defines the unknown expansion

coefficients. Note, all the integrals over  $\varphi$  just equal  $\int_0^{2\pi} d\varphi \cos^2 \varphi = \pi$  and will not be mentioned again. Additional details of the modeling, e.g., the system of equations in explicit form, are presented in Online Resource 1.

To analyze the polarizability dispersion, one needs to solve the resulting system of equations repeatedly for each required wavelength. The polarizability is determined by those expansion coefficients, which correspond to the terms with  $\frac{1}{r^2}$  (the dipole terms). According to that, from Eq. 1a, we obtain the following expression for polarizability  $\alpha$ :

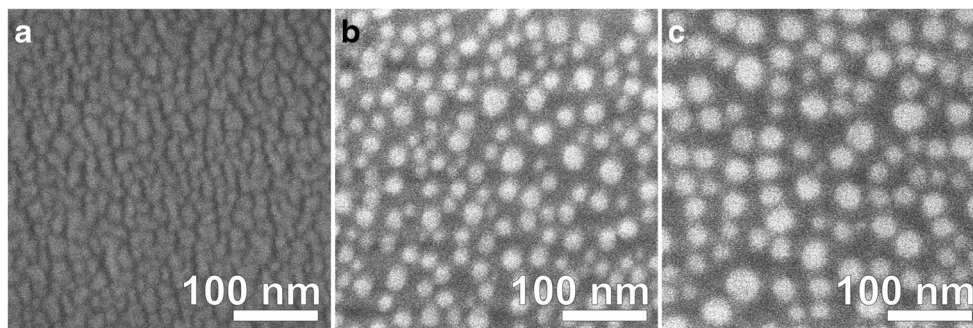
$$\alpha = B_1^1 \left( 1 + \frac{\varepsilon_1 - \varepsilon_2}{\varepsilon_1 + \varepsilon_2} \right) \quad (5)$$

## Results and Discussion

### Scanning Electron Microscopy

The transformation from a percolated gold film (Fig. 2a) to the island structure [27] goes essentially below film melting temperature in accordance with surface diffusion driven dewetting mechanism [33]. Under annealing, initially metastable or unstable [33] film forms a discontinuous network. Generally, the dewetting starts at the film non-uniformities, like holes, which grow and, further, overlap [33]. The non-uniformities of the initial gold film are seen in Fig. 2a; the SEM image of the nanoislands formed from this film after annealing at 500 °C for 2 h is presented in Fig. 2b. Being a transport process, formation of nanoislands strongly depends on temperature, and annealing at elevated temperature should result in bigger nanoislands [27]. Studies of the nanoisland growth at later stages, when Ostwald ripening [34] takes place, allow finding surface diffusion coefficient using the model developed by

**Fig. 2** SEM images of thermally evaporated 5-nm gold film on silica substrate (a), of the same sample, annealed at 500 °C for 120 min (b), of the sample, annealed at 500 °C for 120 min and covered with 50-nm titania layer (c). The effective thickness of all gold films is 5 nm



Sigsbee [35] for 2D process and, if several annealing temperatures are used, the diffusion activation energy [27]. At the stage of Ostwald ripening, smaller nanoislands lose atoms in favor of bigger ones and, finally, rather big—up to several microns in diameter—particles can grow [27]. Unfortunately, our attempts to characterize the shape of the nanoparticles using other than 90° SEM geometry failed because of small size of the nanoparticles and charging samples. This coincides with the observations of Gupta and co-authors [24], who also could not get shape information from SEM measurements using inclined geometry.

Figure 2c presents the SEM image of the sample shown in Fig. 2b after covering with 50 nm of titania. Covering the nanoisland film with titania by ALD provides very uniform distribution of the TiO<sub>2</sub> layer. This means that the cover has the same thickness on the top of the nanoparticles, on their tilted surface, and on the substrate, and that the surface profile formed by the nanoislands becomes smoother very slowly with the increase in the thickness of the ALD layer. The relief of the ALD-covered metal island film (MIF) is very close to the relief of the initial MIF for thinner films, and it stays unsmooth and critically related to the relief of the MIF even up to 200-nm ALD film thicknesses [13].

Analysis of the SEM image of the sample used in further experiments (5-nm gold film on silica substrate annealed at 500 °C for 120 min) allowed deducing mean diameter of the nanoislands and its standard deviation as 17.6 and 4.6 nm, respectively. This evaluation is based on 254 measurements. The histogram of the diameter distribution is presented in Fig. 3.

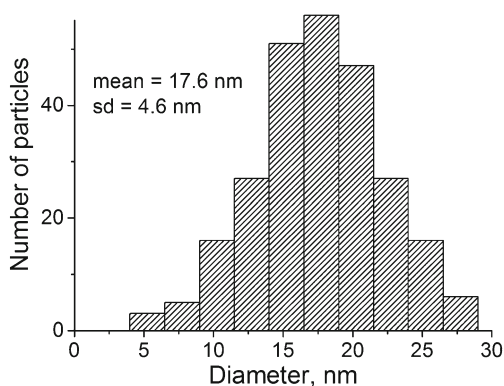


**Fig. 3** Size distribution of the nanoislands formed on silica substrate after annealing of 5-nm gold film at 500 °C for 120 min

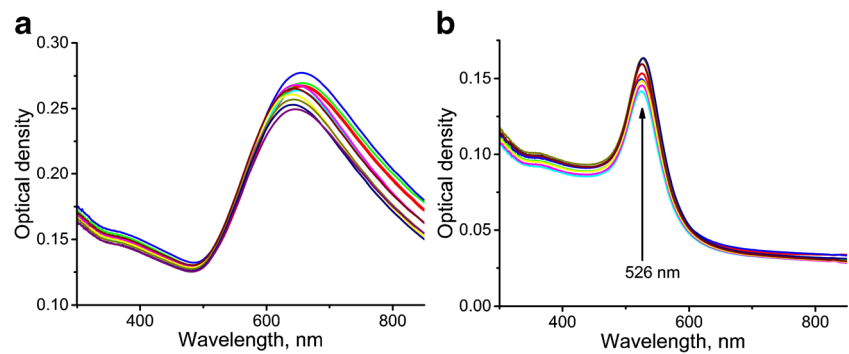
## Absorption Spectra and Ellipsometry

Figure 4a illustrates the absorption spectra of several samples with 5-nm gold film deposited onto silica substrate under the same regime. The absorption peaks lie near 650-nm wavelength. The reproducibility error in the absorption at the resonance wavelength is ~10%. Figure 4b shows the spectra for the same samples annealed at 500 °C for 120 min. The SPR peaks shifted to 530 nm with essentially improved coincidence.

Processing of the ellipsometry data using Tauc-Lorentz formulation [36, 37] allowed us to obtain exact thicknesses of deposited titania layers with 90% confidence limits within ±0.06 nm for the set of six prepared samples. The values of thickness estimated according to number of the deposition cycles and ellipsometry data are presented in Table 1. Index of refraction obtained from the ellipsometry data was  $n = 2.3868$  at 600 nm, imaginary part of the index being negligible.

Figure 5a plots the absorption spectra measured for the samples with 5-nm gold film deposited onto silica substrate, annealed at 500 °C for 120 min and coated with different thicknesses of TiO<sub>2</sub>. The SPR peak is redshifted from 530 to 620 nm with increase of the coating thicknesses. In Fig. 5b, we plotted the dependence of the SPR peak wavelength on the coating thickness together with such dependencies simulated using Eq. 5; the simulated dependence of the SPR position on the truncation angle of uncoated gold nanosphere is presented in the Fig. 5b inset. The latter curve was calculated in the dipole approximation using Johnson and Christy [38] dispersion data for gold. According to this graph, the SPR position in bare truncated nanosphere corresponds to the truncation angle  $\theta_{in}=50^\circ$  (see Fig. 1). This value of the truncation angle provides the distance from the particle center to the substrate surface equal to ~65% of the sphere radius. The theoretical curves for titania-covered nanospheres were calculated for gold nanosphere ( $\theta_{in}=0^\circ$ ) and truncated gold nanosphere with truncation angle  $\theta_{in}=60^\circ$ , both being 8.8 nm in radius and laying on the glass substrate. The experimental points fall between these two curves. In the case of hemispherical particles ( $\theta_{in}=90^\circ$ ), the theoretical curve goes essentially higher than one for  $\theta_{in}=60^\circ$ , and its saturation level corresponds to

**Fig. 4** Absorption spectra of thermally evaporated 5-nm initial gold film on silica substrates (a). Absorption spectra of gold films with effective thickness of 5 nm annealed at 500 °C for 120 min (b) (color online)



**Table 1** Thicknesses of deposited TiO<sub>2</sub> films

Sample	1	2	3	4	5	6
Estimated thickness, nm	3	5	7.5	10	20	30
Ellipsometry data, nm	3.24	3.82	6.76	9.69	18.83	28.25
90% confidence interval, nm	±0.02	±0.02	±0.02	±0.03	±0.04	±0.04

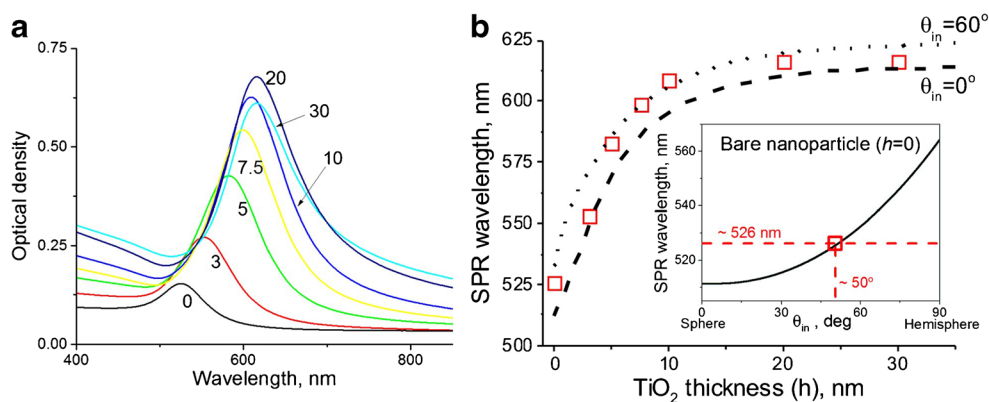
the wavelength of 680 nm. Note that in the dipole approximation, a particle actual size does not directly affect its plasmonic properties, but the relation of coating thickness and the particle radius defines the spectral shift of the SPR. In performed modeling, the substrate and the coating (when applicable) indices were taken independent on wavelength, respectively,  $n_{\text{sub}} = 1.48$  and  $n_{\text{coat}} = 2.4$ , which corresponds to our ellipsometry results at the wavelength of 600 nm. The comparison of experimental data and simulated dependencies allows evaluating of the truncation angle of our nanoparticles as  $\theta_{\text{in}} \sim 50^\circ$ . Thus, measurements of the SPR wavelength of truncated metal nanospheres, both bare and covered with dielectric layers of different thicknesses, allow estimating of the truncation angle.

Figure 5b also illustrates the saturation of the dependence of the resonant wavelength on the coating thickness. This

means that at a certain thickness (according to Fig. 5b it is about 20–30 nm for a particle of 8.8 nm in radius), the induced electric field is almost fully localized in the covering layer and the particle barely “feels” any further increase in the coating thickness.

## Conclusions

The model of plasmonic nanoparticles shaped as a truncated sphere with a coating layer has been developed for the first time. Measured dependence of the surface plasmon resonance wavelength of the gold nanoisland film on the thickness of titania coating has coincided with the dependence calculated for nanoparticles shaped as truncated spheres with the truncation angle of  $\sim 50^\circ$ . We demonstrated that the SPR can be



**Fig. 5** Absorption spectra of gold nanoisland films coated with TiO<sub>2</sub> films of different thicknesses (thickness in nanometer marked near the curves). Before coating, all the samples were annealed at 500 °C for 120 min (a). Experimental (squares) and theoretical thickness dependencies of the surface plasmon resonance wavelength. Theoretical

results are presented for truncated gold nanospheres with different truncation angles  $\theta_{\text{in}}$ . *Inset*: spectral position of the SPR wavelength as a function of bare nanoparticle truncation angle, the square marker denotes the measured wavelength of the SPR (b) (color online)

precisely shifted up to 100 nm towards longer wavelengths by depositing titania layer on the island film. As soon as the SPR position also depends on the truncation angle of the nanoparticles, which, in its turn, can be governed by annealing temperature [24], this broadens the range of the SPR tuning.

**Acknowledgements** This study was supported by the Ministry of Education and Science of the Russian Federation (project #16.1233.2014/K) and by Academy of Finland. S.Ch. acknowledges the support from RFBR Grant No. 16-32-00451. I.R. thanks the grant for support of leading scientific schools #NSh-10235.2016.2. S.Ch. is grateful to Pertti Pääkkönen and Niko Penttinen from the University of Eastern Finland for introductory course on ellipsometry.

## References

- Okamoto T, Yamaguchi I, Kobayashi T (2000) Local plasmon sensor with gold colloid monolayers deposited upon glass substrates. *Opt Lett* 25:372–374. doi:10.1364/OL.25.000372
- Nath N, Chilkoti A (2002) A colorimetric gold nanoparticle sensor to interrogate biomolecular interactions in real time on a surface. *Anal Chem* 74:504–509. doi:10.1021/ac015657x
- Mitsui K, Hanada Y, Kajikawa K (2004) Optical fiber affinity biosensor based on localized surface plasmon resonance. *Appl Phys Lett* 85:4231. doi:10.1063/1.1812583
- Shafer-Peltier KE, Hayner CL, Glucksberg MR, Duyne RP (2003) Toward a glucose biosensor based on surface-enhanced Raman scattering. *J Am Chem Soc* 125:588–593. doi:10.1021/ja028255v
- Abe S, Kajikawa K (2006) Linear and nonlinear optical properties of gold nanospheres immobilized on a metallic surface. *Phys Rev B* 74:035416. doi:10.1103/PhysRevB.74.035416
- Tsuboi K, Abe S, Fukuba S et al (2006) Second-harmonic spectroscopy of surface immobilized gold nanospheres above a gold surface supported by self-assembled monolayers. *J Chem Phys* 125:174703. doi:10.1063/1.2363979
- Xu P, Kang L, Mack NH, Schanze KS et al (2013) Mechanistic understanding of surface plasmon assisted catalysis on a single particle: cyclic redox of 4-aminothiophenol. *Sci Rep* 3:2997. doi:10.1038/srep02997
- Clavero C (2014) Plasmon-induced hot-electron generation at nanoparticle/metal-oxide interfaces for photovoltaic and photocatalytic devices. *Nat Photonics* 8:95–103. doi:10.1038/nphoton.2013.238
- Kim J, Choi H, Nahm C, Park B (2012) Surface-plasmon resonance for photoluminescence and solar-cell applications. *Electron Mater Lett* 8:351–364. doi:10.1007/s13391-012-2117-8
- Kelly KL, Coronado E, Zhao LL, Schatz GC (2003) The optical properties of metal nanoparticles: the influence of size, shape, and dielectric environment. *J Phys Chem B* 107:668–677. doi:10.1021/jp026731y
- Lal S, Link S, Halas NJ (2007) Nano-optics from sensing to waveguiding. *Nat Photon* 1:641–648. doi:10.1038/nphoton.2007.223
- Barnes WL, Dereux A, Ebbesen TW (2003) Surface plasmon sub-wavelength optics. *Nature* 424:824–830. doi:10.1038/nature01937
- Chervinskii S, Matikainen A, Dergachev A, Lipovskii A, Honkanen S (2014) Out-diffused silver island films for surface-enhanced Raman scattering protected with TiO<sub>2</sub> films using atomic layer deposition. *Nanoscale Res Lett* 9:398. doi:10.1186/1556-276X-9-398
- Chen YS, Frey W, Kim S et al (2011) Silica-coated gold nanorods as photoacoustic signal nano-amplifiers. *Nano Lett* 11:348–354. doi:10.1021/nl1042006
- Bayer CL, Chen YS, Kim S et al (2011) Multiplex photoacoustic molecular imaging using targeted silica-coated gold nanorods. *Biomed Opt Express* 2:1828–1835. doi:10.1364/BOE.2.001828
- Daniel MC, Astruc D (2004) Gold nanoparticles: assembly, supramolecular chemistry, quantum-size-related properties, and applications toward biology, catalysis, and nanotechnology. *Chem Rev* 104:293–346. doi:10.1021/cr030698+
- Xing R, Jiao T, Yan L et al (2015) Colloidal gold–collagen protein core–shell nanoconjugate: one-step biomimetic synthesis, layer-by-layer assembled film, and controlled cell growth. *Appl Mater Interfaces* 7:24733–24740. doi:10.1021/acsami.5b07453
- Adamov M, Perović B, Nenadović T (1974) Electrical and structural properties of thin gold films obtained by vacuum evaporation and sputtering. *Thin Solid Films* 24:89–100. doi:10.1016/0040-6090(74)90254-5
- Worsch C, Wisniewski W, Kracker M, Rüssel C (2012) Gold nanoparticles fixed on glass. *Appl Surf Sci* 8:8506–8513. doi:10.1016/j.apsusc.2012.05.010
- Švorčík V, Kvítek O, Lyutakov O, Siegel J, Kolská Z (2011) Annealing of sputtered gold nano-structures. *Appl Phys A Mater Sci Process* 8:747–751. doi:10.1007/s00339-010-5977-5
- Porath D, Millo O (1996) Scanning tunneling microscopy studies and computer simulations of annealing of gold films. *J Vacuum Sci Technol* 8:30–37. doi:10.1116/1.588467
- Müller CM, Spolenak E (2010) Microstructure evolution during dewetting in thin Au films. *Acta Mater* 8:6035–6045. doi:10.1016/j.actamat.2010.07.021
- Worsch C, Wisniewski W, Kracker M, Rüssel C (2012) Gold nanoparticles fixed on glass. *Appl Surf Sci* 258:8506–8513. doi:10.1016/j.apsusc.2012.05.010
- Gupta G, Tanaka D, Ito Y et al (2009) Absorption spectroscopy of gold nanoisland films: optical and structural characterization. *Nanotechnology* 20:025703. doi:10.1088/0957-4484/20/2/025703
- Tian F, Bonnier F, Casey A, Shanahan AE, Byrne HJ (2014) Surface enhanced Raman scattering with gold nanoparticles: effect of particle shape. *Anal Methods* 6:9116–9123. doi:10.1039/x0xx00000x
- Scherbak SA, Shustova OV, Zhurikhina VV, Lipovskii AA (2015) Electric properties of hemispherical metal nanoparticles: influence of the dielectric cover and substrate. *Plasmonics* 10:519–527. doi:10.1007/s11468-014-9836-7
- Ruffino F, Torrisi V, Marletta G, Grimaldi MG (2011) Atomic force microscopy investigation of the kinetic growth mechanisms of sputtered nanostructured Au film on mica: towards a nanoscale morphology control. *Nanoscale Res Lett* 6:112. doi:10.1186/1556-276X-6-112
- Zhang M, Lin G, Dong C, Wen L (2007) Amorphous TiO<sub>2</sub> films with high refractive index deposited by pulsed bias arc ion plating. *Surf Coat Technol* 201:7252–7258. doi:10.1016/j.surfcoat.2007.01.043
- Saleem MR, Honkanen S, Turunen J (2014) Thermal properties of TiO<sub>2</sub> films fabricated by atomic layer deposition. *IOP Conf Ser: Mater Sci Eng* 60:012008. doi:10.1088/1757-899X/60/1/012008
- Wind MM, Vlioger J, Bedeaux D (1987) The polarizability of a truncated sphere on a substrate I. *Physica A* 141:33–57. doi:10.1016/0378-4371(87)90260-3
- Leskela M, Ritala M (2003) Atomic layer deposition chemistry: recent developments and future challenges. *Angew Chem Int Ed* 42:5548–5554. doi:10.1002/anie.200301652
- Mayer SA (2007) *Plasmonics: fundamentals and applications*. Springer, Bath
- Thompson CV (2012) Solid-state dewetting of thin films. *Annu Rev Mater Res* 42:399–434. doi:10.1146/annurev-matsci-070511-155048

34. Ostwald W (1897) Studien über die Bildung und Umwandlung fester Körper. *Z Phys Chem* 22:289–330
35. Sigsbee RA (1971) Adatom capture and growth rates of nuclei. *J Appl Phys* 42:3904–3915. doi:[10.1063/1.1659705](https://doi.org/10.1063/1.1659705)
36. Jellison GE, Modine FA (1996) Parameterization of the optical functions of amorphous materials in the interband region. *Appl Phys Lett* 69:371–374. doi:[10.1063/1.118064](https://doi.org/10.1063/1.118064)
37. Von Blanckenhagen B, Tonova D, Ullmann J (2002) Application of the Tauc–Lorentz formulation to the interband absorption of optical coating materials. *Appl Opt* 41:3137–3141. doi:[10.1364/AO.41.003137](https://doi.org/10.1364/AO.41.003137)
38. Johnson PB, Christy RW (1972) Optical constants of the noble metals. *Phys Rev B* 6:4370. doi:[10.1103/PhysRevB.6.4370](https://doi.org/10.1103/PhysRevB.6.4370)